https://doi.org/10.1016/j.jallcom.2019.06.097

The prominent combination of ultrahigh strength and superior tensile plasticity in Cu-Zr nanoglass connected by oxide interfaces: A molecular dynamics study

Mao Zhang[a]

Qiao-Min Li[b]

Jia-Cheng Zhang[b]

Guang-Ping Zheng[a, *]

mmzheng@polyu.edu.hk

Xin-Yun Wang[b, **]

wangxy_hust@hust.edu.cn

[a]Department of Mechanical Engineering, The Hong Kong Polytechnic University, Hung Hom, Kowloon, 999077, Hong Kong, China

[b]State Key Laboratory of Materials Processing and Die & Mould Technology, Huazhong University of Science and Technology, 1037 Luoyu Road, Wuhan, 430074, China

*Corresponding author.

**Corresponding author.

Abstract

A novel Cu–Zr nanoglass consisting of glassy nano-cells connected by oxide interfaces is proposed. Compared to conventional nanoglasses, the novel oxide-connected nanoglass presents ultrahigh tensile strength and superior tensile plasticity at ambient temperature. Subjected to tensile loading, the oxide interfaces are found to promote the nucleation of shear transformation zones (STZs) due to the existence of excess free volume. Meanwhile, the strong bonding between metallic and oxygen atoms in the oxide interface makes it difficult for STZs to propagate through. Thus, the STZs are effectively proliferated and confined inside the cell interior without any mature shear band (SB) formed. The results provide new ideas for toughening metallic glasses with a decent combination of plasticity and strength, thus making it possible to overcome the longstanding strength-ductility trade-off dilemma.

Keywords: Nanoglass; Oxidation; Interface; Shear transformation; Molecular dynamics

1 Introduction

Metallic glasses (MGs) have already been widely recognized with promising application prospects as functional and engineering materials, since they possess the mechanical strength close to the theoretical strength of solids in their glassy state as well as the superior plasticity in their supercooled liquid state [1,2]. However, due to the localization of plastic strains and the quick propagation of individual shear bands (SBs), MGs present significant brittleness at ambient temperatures, which strictly limits their structural applications [3]. Hence, numerous approaches have been developed to toughen MGs, aiming to possess an enhanced plasticity at ambient temperatures while reserving their high mechanical strength [4,5].

The introduction of heterogeneous interfaces into MGs has been validated to be effective in promoting the nucleation of multiple SBs and hindering the immoderate propagation of them [6–9]. Nanoglass (NG), which consists of nanoscale glassy grains connected by glass/glass interfaces is one of the most typical applications of this concept [10–12]. Available studies have demonstrated that the soft glass/glass interfaces can act as the preferred nucleation regions for SBs, and promote the proliferation of multiple SBs [13]. Thus, the plasticity of NGs can be significantly improved, especially, when the average grain size reduces to a critical value, the plastic deformation pattern transforms from localized shear banding to homogenous superplastic flow [14].

However, the improvement of plasticity is usually achieved by the sacrifice of strength, which is known as the longstanding strength-ductility trade-off dilemma [15]. Admit of no exception, as reported in Ref. [14], although

$Cu_{50}Zr_{50}$ NG with grains smaller than 5 nm can deform in a superplastic way, its peak strength is ~2.1 GPa, while that of $Cu_{50}Zr_{50}$ MG is ~3.3 GPa under the same condition. The softening in NGs is caused by the large volume fraction of loosely packed interfaces, which is the intrinsic feature of NGs and prerequisite of enhanced plasticity [11]. Hence, it becomes very challenging but meaningful to find some way to increase the deformation resistance of the glass/glass interfaces while maintaining their loose packing structures.

Oxygen interstitials can strengthen crystalline metals via pinning dislocation propagation and promoting dislocation multiplication [16–18]. Although the plastic deformation of MGs is intermediated via SBs, instead of dislocations, if the excessive propagation of SBs can be hindered, it is also possible to increase the deformation resistance. Moreover, it has already been reported that a suitable degree of oxidation is beneficial to the improvement of microhardness and corrosion resistance of Zr-based bulk metallic glass (BMG) [19]. Hence, we proposed a novel type of NG which consists of glassy cells connected by glassy oxide interfaces, named as ONG, aiming to improve the deformation resistance by hindering the propagation of SBs through the oxide interfaces while promoting the multiplication of SBs. Based on molecular dynamics (MD) approaches, the global mechanical properties and atomic structures of the proposed ONG were investigated, with the corresponding strengthening mechanisms discussed.

2 Methods

At the beginning, a model of $Cu_{64}Zr_{36}$ MG was constructed via quenching the $Cu_{64}Zr_{36}$ melt with 148812 atoms from 2000 K to 50 K at a cooling rate of 10 K/ps under zero external pressure (NPT ensemble). To reduce the computational costs, in the construction of $Cu_{64}Zr_{36}$ MG model, the embedded atom model (EAM) potential was utilized [20]. Periodic boundary conditions (PBCs) were applied along all three directions.

The MG model was divided into four (equivalent based on PBCs) hexagonal glassy cells by a gap network with a width of 8.5 Å. Cu and Zr atoms inside the gap network were deleted or replaced by O atoms, resulting in a $Cu_{64}Zr_{36}$ NG with 134876 atoms and a $Cu_{59}Zr_{33}O_8$ ONG with 148812 atoms, respectively. The charge-optimized many-body (COMB3) potential was employed to describe the interatomic interactions among Cu, Zr, and O atoms [21]. To avoid possible crystallization, the NG and ONG models were consolidated by isothermal equilibration under a hydrostatic pressure of 1 bar and at 400, 500, 600, and 700 K for 500 ps, respectively [22]. After consolidation, the system was cooled down to 300 K within 500 ps and equilibrated at 300 K for another 500 ps. Thus, the empty gap network in the NG was eliminated while interdiffusion took place between the oxygen gap network and cell interior in the ONG, as shown in Fig. 1. The grain sizes of those hexagonal glassy cells are about 115–120 Å, and the oxide interfaces are found to be much rough with a thickness of 16.2–22.5 Å, depending on the consolidation temperature. To quickly dissipate the heat generated by oxidation during consolidation, the Berendsen thermostat and barostat were utilized to control the temperature and pressure, with the positions and velocities of atoms updated by the microcanonical ensemble (NVE) [23] (see Fig. 2).

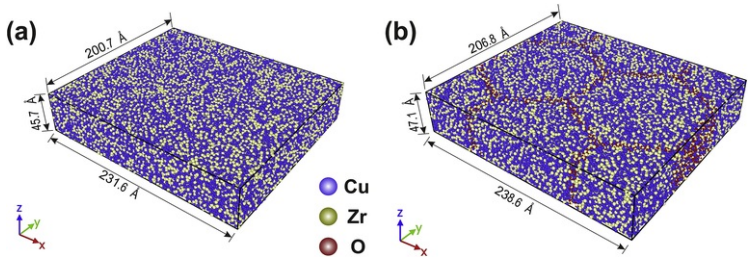

Fig. 1 (a) $Cu_{64}Zr_{36}$ NG and (b) $Cu_{59}Zr_{33}O_8$ ONG structures consolidated at 600 K.

alt-text: Fig. 1

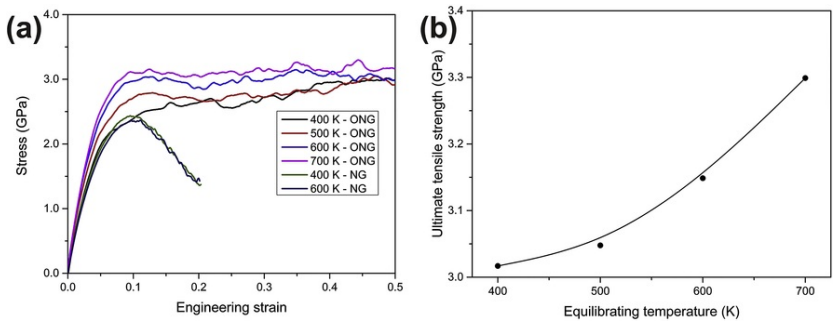

Fig. 2 (a) Engineering strain-stress curves of ONGs and NGs consolidated at different temperatures, (b) influence of consolidation temperature on the ultimate tensile strengths of ONGs.

alt-text: Fig. 2

Uniaxial tension was applied on the *x*-direction, with a constant stretching velocity of 0.01 Å/ps (corresponding to an initial strain rate of 4.35×10^{-5} ps^{-1}). During tension, the temperature was kept at 300 K by using the Berendsen thermostat, with the velocities and positions of atoms updated by the NVE ensemble. PBCs were also applied on all three directions.

MD simulations were all performed by using Large-scale Atomic/Molecular Massive Parallel Simulator (LAMMPS) [24]. The simulation timestep was all set as 1 fs. Simulation results were processed and visualized by using self-developed Python codes and the OVITO software package [25].

3 Results and discussions

Fig. 1(should be Fig. 2a)a shows the engineering strain-stress curves (flow curves) of ONGs and NGs subjected to uniaxial tension. After a linear elastic stage, the curves rise nonlinearly and reach their ultimate tensile strength (UTS). For the NGs, their curves experience notable drop after UTS, indicating the massive formation, propagation and localization of SBs [26]. The deformation behavior of $Cu_{64}Zr_{36}$ NGs is akin to those of $Cu_{50}Zr_{50}$ NGs with grain sizes greater than 10 nm reported in Ref. [14]. The strain-stress curves of NGs consolidated at 400 K and 600 K show little difference, indicating that the consolidation temperature has limited influence on the mechanical properties of NGs.

On the contrary, for all ONGs, their curves show no notable reduction even after reaching an engineering strain of 0.5 (the maximum engineering strain simulated here), which demonstrates superior plasticity. The UTSs of ONGs are much higher than those of NGs prepared under the same condition. For example, the UTS of NG consolidated at 600 K is about 2.44 GPa, while that of ONG consolidated at 600 K is 3.14 GPa, with an increase magnitude of 28.7%. According to available experimental data, the tensile strengths of Cu–Zr-based bulk MGs are mostly around 2.0 GPa, and approach to 3.0 GPa after the specimen size reducing to submicron scale [27]. Meanwhile, the UTS of the ONG consolidated at 700 K reaches 3.3 GPa. Hence, it is implied that the ONG proposed here can obtain superior plasticity without sacrificing its strength, instead, the strength can even be further enhanced. Moreover, the elastic limit lies around 5%, which is notably high comparing to bulk MGs [28]. The UTSs of ONGs show strong temperature-dependence, that is, they increase notably with the increase of consolidation temperature (Fig. 1b(should be Fig. 2b)). Undoubtedly, the obvious temperature-dependence of ONG mechanical properties stems from the strong temperature-dependence of metallic glass oxidation behaviors [29,30].

To understand the origin of the superior plasticity and ultrahigh strength of ONGs, the local shear strain η^{Mises} distribution during uniaxial tension was characterized, as shown in Fig. 3. It is obvious that shear transformation zones (STZs) preferentially nucleate in the vicinity of oxide interfaces in the early stage (Fig. 3a, d, g and j), indicating that the oxide interface can promote the initiation of STZs [31].

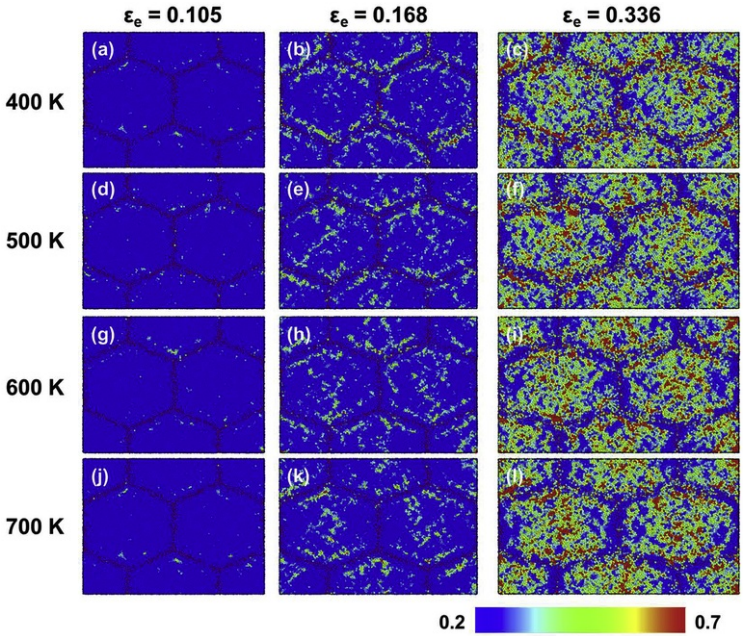

Fig. 3 Distribution of local shear strain in ONGs during tension. Cu and Zr atoms are colored according to their local shear strain magnitudes, while O atoms are colored in dark red to indicate the oxide interface position during tension. (For interpretation o the references to color in this figure legend, the reader is referred to the Web version of this article.)

alt-text: Fig. 3

With tensile strain rising, the STZs near the interfaces interconnect with each other and distribute parallelly to the interfaces. At the meantime, STZs also nucleate in the interior of cells (Fig. 3b, e, h and k). STZs in the interior of cells further develop and result in a highly dense and nearly homogenous distribution of STZs there, while the STZ distribution inside the oxide interfaces is rare (Fig. 3c, f, i and l). This strong deviation implies that in the late stage, the deformation is mainly accommodated by the STZ formation in the cell interior while the propagation of STZs through the oxide interfaces is strongly suppressed. Since the propagation of STZs is effectively confined inside the cell, it becomes difficult for STZs to develop into SBs, although the size of cells approaches to the critical thickness of SBs, which has been reported to be 50–112 Å [32]. It also should be noted that with the increase of consolidated temperature, the density of STZs inside the oxide interfaces reduces, i.e., the confinement effect of oxide interface on STZ propagation becomes stronger.

The deviation of local shear strain η^{Mises} distribution between the cell interior and oxide interface can be quantitively characterized by the shear strain localization factor defined by Cheng et al. [33], that is, $\psi = \sqrt{\frac{1}{N}\sum_{i=1}^{N}\left(\eta_i^{\mathrm{Mises}} - \eta_{av}^{\mathrm{Mises}}\right)^2}$, where η_i^{Mises} is the local shear strain of the i-th atom, $\eta_{av}^{\mathrm{Mises}}$ is the average shear strain of all atoms in the system, and N is the total number of atoms. A higher value of ψ indicates a more significant localization of deformation. The ψ values of ONGs subjected to uniaxial tension are plotted in Fig. 4a, while Fig. 4b shows the normalized shear strain localization factor ψ_{normal} , i.e., $\psi_{normal} = \psi/\eta_{av}^{\mathrm{Mises}}$. For all ONGs, ψ increases with the increase of global engineering strain. Meanwhile, the evolution of ψ_{normal} shows some difference, that is, for ONGs consolidated at 600 K and 700 K, ψ_{normal} rises monotonously with global strain increasing, indicating that the confinement effect of the oxide interface becomes stronger and STZs are mainly formed in the cell interior under this condition. On the contrary, ψ_{normal} of the ONG consolidated at 500 K first decreases and then increases, while that for the ONG consolidated at 400 K presents a monotonous reduction trend during tension. It also should be noted that, at global tensile strains lower than 0.168, increasing the consolidation temperature will reduce the localization degree, while for global tensile strain higher than 0.168, the influence of consolidation temperature becomes opposite. These changes will be discussed in the following sections.

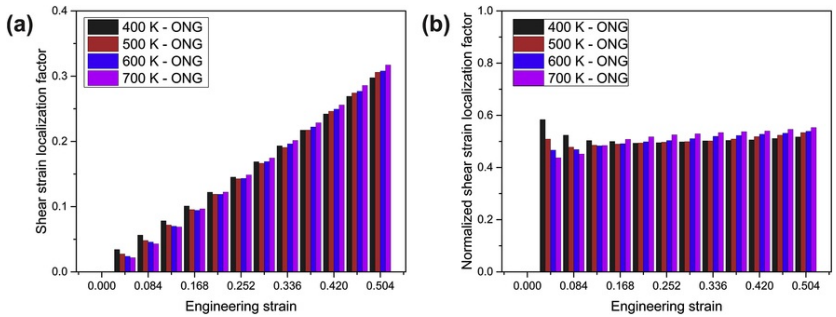

Fig. 4 (a) Shear strain localization factors and (b) the corresponding normalized values of ONGs subjected to tensile strain.

alt-text: Fig. 4

The fractions of shear transformed atoms are calculated to reveal the roles of each atom type during shear transformation as well as the influencing mechanism of consolidation temperature. Fig. 5a and d compare the fraction of each atom type in STZs formed in ONGs consolidated at 500 K and 700 K, respectively. It is demonstrated that the fraction of O atoms in STZs is the highest at the beginning of tension and continuously reduces with global strain rising. Meanwhile, the fractions of Cu and Zr atoms in STZs rise gradually. Hence, it is implied that STZs preferentially initiate in O-rich regions, i.e., the oxide interfaces and surrounding regions, while the shear transformation in the cell interior becomes the dominant after global tensile strain reaches ~0.1. Increasing the consolidation temperature results in a higher fraction of O atoms in SZTs at the beginning, but this influence becomes negligible after the global strain exceeds 0.1 and the atomic composition in STZs is close to the global atomic composition.

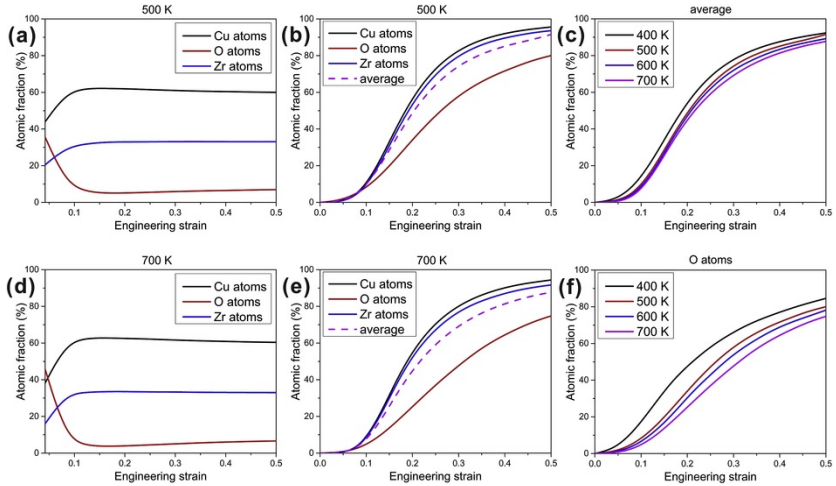

Fig. 5 (a, d) The per-type fraction of atoms in STZs formed in ONGs consolidated at 500 K and 700 K; (b, e) the fraction of shear transformed atoms ($\eta^{\mathrm{Mises}} \geq 0.2$ in each atom type in ONGs consolidated at 500 K and 700 K; (c) the fraction of shear transformed atoms averaged over each atom type in ONGs consolidated at different temperatures; and (f) the fraction of shear transformed O atoms among all O atoms in ONGs consolidated at different temperatures.

alt-text: Fig. 5

Fig. 5b and e shows the fractions of shear transformed atoms in each atom type, i.e., N_i^{ST}/N_i, where N_i is the total number of the i-th atom type, and N_i^{ST} is number of shear transformed i-type atoms. The average fraction refers to the ratio of the number of all shear transformed atoms to the total number of atoms in the whole system. It is demonstrated that most of the Zr and Cu atoms (higher than 90%) are shear transformed when the global strain reaches 0.5, meanwhile, the fraction of O atoms experienced shear transformation is far lower than those of Zr and O atoms, which is 80.3% at 500 K and 75.1% at 700 K at a global strain of 0.5. Fig. 5c and f compare the influence of consolidation temperature on the fractions of shear transformed atoms. It is implied that with the increase of consolidation temperature, the averaged fraction of shear transformed atoms decreases gradually, but the magnitude is small. Meanwhile, that of shear transformed O atoms experiences notable decrease, indicating strong temperature-sensitivity, especially at low global strain ranges. In combination with Figs. 3 and 5, we can also find that STZs

preferentially initiate mainly in the vicinity of oxide interface, instead of inside it.

In Cu–Zr MG systems, the full icosahedral (FI) clusters (Voronoi polyhedra with index of <0 0 12 0>) has been recognized as the prominent structural features [33]. Since FIs, especially Cu-centered FIs, have high packing density and strong shear resistance, they are crucial for the elasticity and plasticity of MGs. The reduction of FI amounts inevitably leads to a stronger propensity of STZ induced plasticity [14]. Voronoi polyhedra analyses were conducted by using the OVITO software, which can generate the Voronoi indices of each atom. The results were further processed for statistical analysis through self-developed Python codes. Fig. 6 compares the evolution of FI amounts during uniaxial tension of ONGs consolidated at 500 K and 700 K, respectively. It is obvious that the FIs are mainly Cu-centered, while no O-centered FI exists, implying that FIs mainly distribute in the cell interior. Before tension, the ONG consolidated at 700 K has more FIs than that consolidated at 500 K, which will contribute to the higher UTS. With global strain rising, the amount of FIs drops and reaches a relatively stable value after the global strain exceeding 0.25. The reduction of FIs allows the initiation of more STZs in the cell interior, which bear more plastic strain in the later deformation stage.

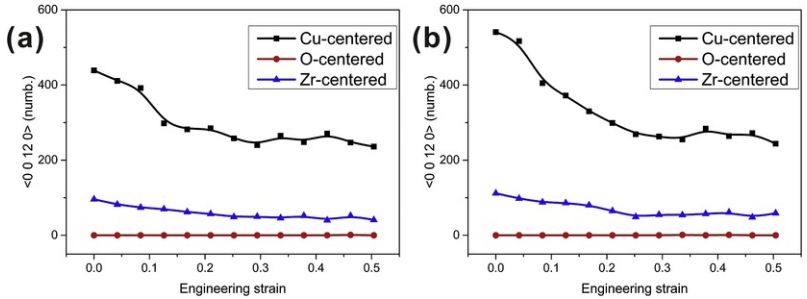

Fig. 6 The number of full icosahedra (Voronoi index of <0 0 12 0>) in ONGs consolidated at (a) 500 K and (b) 700 K.

alt-text: Fig. 6

As stated above, the oxide interface plays a significant role in the deformation of ONGs. Hence, this section focuses on the oxide interface structure and its evolution during tension. Fig. 7a shows an enlarged view of the oxide interface. We can find that the interface is rough, and its thickness is fluctuant. For the simplity and consistency of analysis, the horizontal distance between the leftmost and rightmost O atoms is set as the oxide interface thickness, as illustrated in the figure. Fig. 7b shows the sampling region used in this section, which is a slab region locates in the middle of the *y*-direction with a thickness of 20% of the *y*-direction length. Thus, the sampling region is subjected to purely uniaxial tensile strain during the whole process.

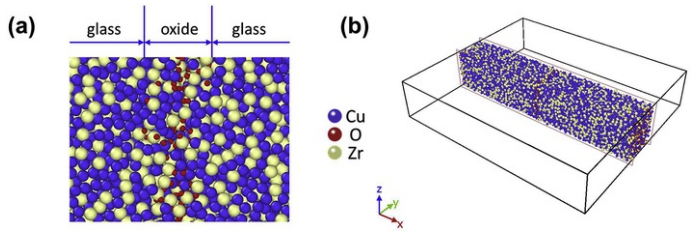

Fig. 7 Schematic of (a) the oxide interface and (b) the sampling region in ONGs.

alt-text: Fig. 7

Fig. 8a shows the oxide interface thickness t_{ox} of ONGs, which all increase with the increase of global tensile strain, but their variation tendency deviates. To better elucidate the response of oxide interface to global strain, we define the local strain of oxide interface as: $\varepsilon_{ox}^{local} = \frac{t_{ox}^{\varepsilon_e} - t_{ox}^{0}}{t_{ox}^{0}}$, where $t_{ox}^{\varepsilon_e}$ is the thickness of oxide interface at a global strain of $\varepsilon_{e,}$ and t_{ox}^{0} is the initial oxide interface thickness. Fig. 8b shows the deviation between the local strain ε_{ox}^{local} and global strain ε_e, which is defined as $\left(\varepsilon_{ox}^{local} - \varepsilon_e\right)/\varepsilon_e$. It is interesting to find that the ONG consolidated at 400 K differs greatly from the rest ONGs, that is, the local-global deviation of the former one mostly lies above zero, while those of the latter ones are all below zero. A negative local-global deviation value means that the oxide interface bears less plastic strain, i.e., plastic strain is mainly achieved by the interior of cells. Meanwhile, the positive local-global deviation value of the ONG consolidated at 400 K implies that the oxide interface bears more tensile strain than the glass interior under this condition.

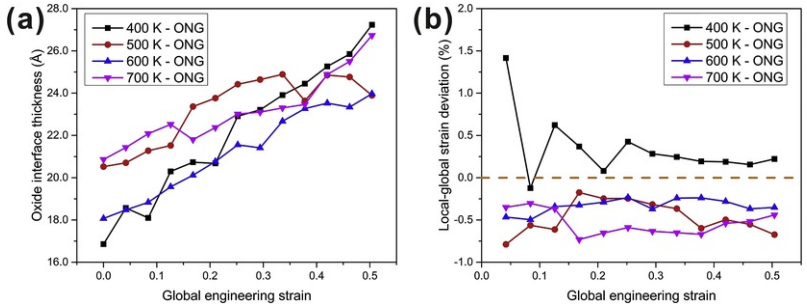

Fig. 8 (a) Oxide interface thickness and (b) local-global strain deviation in ONGs consolidated at different temperatures.

alt-text: Fig. 8

As aforementioned, the role of oxide interface playing during the ONG plastic deformation can be categorized into two aspects: promoting the initiation of STZs in the vicinity of oxide interface and confining the propagation of STZs through the interface.

The former effect has already been well explained by some available studies, which attribute it to the high excess free volume in the interfacial regions [34,35]. Fig. 9 shows the distribution of excess free volume across the oxide interface, while Fig. 10 presents the corresponding elemental distribution. The ONGs proposed in this study also have a high excess free volume in the interfacial regions. For the ONG consolidated at 400 K, there is a sharp peak value of excess free volume around Zr atoms in the middle of the interface (Fig. 9a and b). This is possibly caused by the insufficient delocalization of excess free volume at the relatively low consolidation temperature [10]. The higher content of free volume can enhance the formation of more STZs therein, which can explain the positive local-global strain deviation presented in Fig. 8b as well as the abundant occurrence of STZs in Fig. 3a [36,37]. With the increase of consolidation temperature, the delocalization of excess free volume during consolidation enhances, with the peak content reducing while the region with significant free volume content expanding. Moreover, the delocalization degree further enhances during plastic deformation.

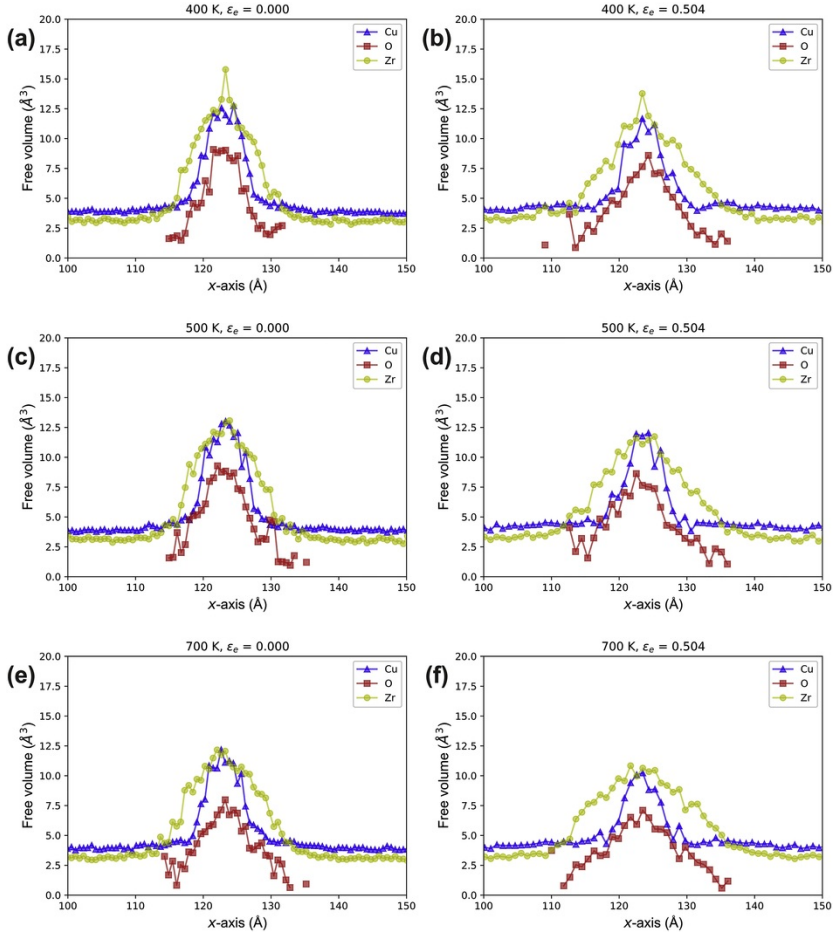

Fig. 9 Distribution of excess free volume across the oxide interface in ONGs (a) consolidated at 400 K and undeformed, (b) consolidated at 400 K and reaching engineering strain of 0.504, (c) consolidated at 500 K and undeformed, (d) consolidated at 500 K and reaching engineering strain of 0.504, (e) consolidated at 700 K and undeformed, and (f) consolidated at 700 K and reaching engineering strain of 0.504.

alt-text: Fig. 9

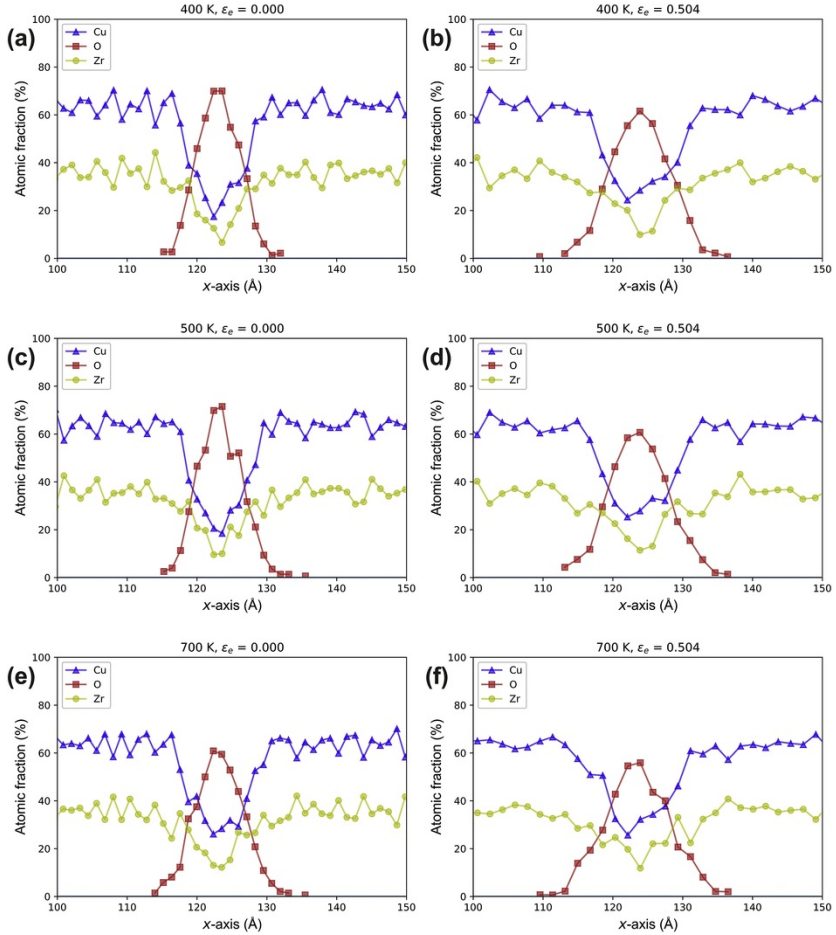

Fig. 10 Distribution of atomic fractions across the oxide interface in ONGs (a) consolidated at 400 K and undeformed, (b) consolidated at 400 K and reaching engineering strain of 0.504, (c) consolidated at 500 K and undeformed, (d) consolidated at 500 K an reaching engineering strain of 0.504, (e) consolidated at 700 K and undeformed, and (f) consolidated at 700 K and reaching engineering strain of 0.504.

alt-text: Fig. 10

As for the confinement effect of the oxide interface on the propagation of STZs, we can explain it in the view of atomic bond dissociation. Table 1 lists the bond dissociation energies of the four major bonds in the ONG system discussed here. Comparing to the M-M (M stands for metal) bonds, the bond dissociation energies of M − O bonds are significantly improved, that is to say, it requires more energy to break these bonds to realize the shear transformation process [38,39]. Thus, after introducing the oxide interface, the propagation of STZs through the interface becomes more difficult, resulting in strong confinement effect. Moreover, the initiation of STZs in regions with high content of O atoms also becomes hard. Therefore, STZs preferentially initiate in the vicinity of the oxide interface, where the free volume content is relatively high, and the content of O atoms is relatively low.

Table 1 Bond dissociation energies for the Cu–Zr–O system [40].

alt-text: Table 1

Bond type	Cu–Cu	Cu–O	Zr–Zr	Zr–O
Dissociation energy (kJ/mol)	201	287.4 ± 11.6	298.2 ± 0.1	766.1 ± 10.6

According to Fig. 10a, c, and e, the atomic compositions in the middle of oxide interface are $Cu_{23.3}Zr_{6.7}O_{70.0}$, $Cu_{20.6}Zr_{9.6}O_{69.8}$, and $Cu_{26.1}Zr_{13.0}O_{60.9}$ for ONGs consolidated at 400 K, 500 K and 700 K, respectively. That is, the O content gradually reduces with the increase of consolidation temperature, due to the enhanced diffusivity at elevated temperatures [41]. For the interfacial region with a higher fraction of O, the corresponding fractions of Zr and Cu are lower. Thus, the number of effective $M-O$ bonds is reduced, and the confinement effective of the oxide interface on STZs is weakened. With the consolidation temperature improved, O atoms diffuse farer and more $M-O$ bonds are formed inside, thus, the oxide interface becomes wider and stronger. After subjected to uniaxial tension, the central atomic compositions in the oxide interfaces become $Cu_{28.5}Zr_{9.9}O_{61.6}$, $Cu_{27.9}Zr_{11.4}O_{60.7}$, and $Cu_{32.2}Zr_{11.9}O_{55.9}$ respectively, resulting from the further diffusion of atoms enhanced by external tensile loading [42].

4 Conclusions

This work proposes a novel Cu–Zr nanoglass consisting of glassy nano-cells connected by oxide interfaces, named as ONG, based on molecular dynamics simulations. It is found that the ONG exhibits a superior combination of ultrahigh mechanical strength and ductility, that is, the ONG presents superior plasticity even after the tensile strain exceeds 0.5, while its tensile strength is far greater than those of conventional bulk MGs. Due to the high contents of excess free volume in the interfacial regions, massive STZs are found to form in the vicinity of the oxide interface. Meanwhile, attributing to the strong bonding between metallic and oxygen atoms, it is difficult for STZs to propagate through the oxide interface, as well as initiate inside the interface. Thus, shear transformation is strictly confined in the interior of glassy cells, without any mature SB formed. This novel material is promising to overcome the longstanding strength-ductility trade-off dilemma.

Conflicts of interest

The authors declare no competing interest.

Acknowledgments

This work was supported by National Science Fund for Distinguished Young Scholars of China (grant number 51725504), National Natural Science Foundation of China (grant number 51705168, 51805181), Research Grants Council of the Hong Kong Special Administrative Region, China (PolyU152607/16E), and China Postdoctoral Science Foundation (grant number 2017M610473). Computations are performed on Tianhe-2 in National Supercomputer Center in Guangzhou.

Appendix A. Supplementary data

Supplementary data to this article can be found online at https://doi.org/10.1016/j.jallcom.2019.06.097.

References

[1] C. Suryanarayana and A. Inoue, Bulk Metallic Glasses, 2011, CRC Press; Boca Raton.

[2] N. Li, X. Xu, Z. Zheng and L. Liu, Enhanced formability of a Zr-based bulk metallic glass in a supercooled liquid state by vibrational loading, *Acta Mater.* **65**, 2014, 400–411.

[3] B.A. Sun and W.H. Wang, The fracture of bulk metallic glasses, *Prog. Mater. Sci.* **74**, 2015, 211–307.

[4] W. Guo and H. Kato, Development of in-situ β-Ti reinforced Be-free Ti–based bulk metallic glass matrix composites, *J. Alloy. Comp.* **714**, 2017, 120–125.

[5] W. Guo, H. Kato, R. Yamada and J. Saida, Fabrication and mechanical properties of bulk metallic glass matrix composites by in-situ dealloying method, *J. Alloy. Comp.* **707**, 2017, 332–336.

[6] D.C. Hofmann, J. Suh, A. Wiest, M. Lind, M.D. Demetriou and W.L. Johnson, Development of tough, low-density titanium-based bulk metallic glass matrix composites with tensile ductility, *Proc. Natl. Acad. Sci. U. S. A* **105**, 2008, 20136–20140.

[7] Y. Wang, J. Li, A.V. Hamza and T.W. Barbee, Jr., Ductile crystalline-amorphous nanolaminates, *Proc. Natl. Acad. Sci. U. S. A* **104**, 2007, 11155–11160.

[8] G. He, J. Eckert, W. Loser and L. Schultz, Novel Ti-base nanostructure-dendrite composite with enhanced plasticity, *Nat. Mater.* **2**, 2003, 33–37.

[9] J.J. Lewandowski, M. Shazly and A.S. Nouri, Intrinsic and extrinsic toughening of metallic glasses, *Scripta Mater.* **54**, 2006, 337–341.

[10] H. Gleiter, Our thoughts are ours, their ends none of our own: are there ways to synthesize materials beyond the limitations of today?, *Acta Mater.* **56**, 2008, 5875–5893.

[11] Z.D. Sha, P.S. Branicio, Q.X. Pei, Z.S. Liu, H.P. Lee, T.E. Tay and T.J. Wang, Strong and superplastic nanoglass, *Nanoscale* **7**, 2015, 17404–17409.

[12] N. Chen, D.V. Louzguine-Luzgin and K. Yao, A new class of non-crystalline materials: nanogranular metallic glasses, *J. Alloy. Comp.* **707**, 2017, 371–378.

[13] D. Sopu, Y. Ritter, K. Albe and H. Gleiter, Deformation behavior of bulk and nanostructured metallic glasses studied via molecular dynamics simulations, *Phys. Rev. B* **83**, 2011, 100202(R).

[14] S. Adibi, Z. Sha, P.S. Branicio, S.P. Joshi, Z. Liu and Y. Zhang, A transition from localized shear banding to homogeneous superplastic flow in nanoglass, *Appl. Phys. Lett.* **103**, 2013, 211905.

[15] Y. Wei, Y. Li, L. Zhu, Y. Liu, X. Lei, G. Wang, Y. Wu, Z. Mi, J. Liu, H. Wang and H. Gao, Evading the strength-ductility trade-off dilemma in steel through gradient hierarchical nanotwins, *Nat. Commun.* **5**, 2014.

[16] H. Conrad, Effect of interstitial solutes on the strength and ductility of titanium, *Prog. Mater. Sci.* **26**, 1981, 123-403.

[17] M. Jo, P.P. Madakashira, J. Suh and H.N. Han, Effect of oxygen and nitrogen on microstructure and mechanical properties of vanadium, *Mater. Sci. Eng., A* **675**, 2016, 92–98.

[18] Z. Lei, X. Liu, Y. Wu, H. Wang, S. Jiang, S. Wang, X. Hui, Y. Wu, B. Gault, P. Kontis, D. Raabe, L. Gu, Q. Zhang, H. Chen, H. Wang, J. Liu, K. An, Q. Zeng, T. Nieh and Z. Lu, Enhanced strength and ductility in a high-entropy alloy via ordered oxygen complexes, *Nature* **563**, 2018, 546–550.

[19] M. Zhang, D. Yao, Z. Cao, P. Li, P. Zhou and X. Wang, Influence of oxidation on the performance of Zr55Cu30Al10Ni5 BMG, *Intermetallics* **79**, 2016, 20–27.

[20] Y. Kim and B. Lee, A modified embedded-atom method interatomic potential for the Cu-Zr system, *J. Mater. Res.* **23**, 2008, 1095–1104.

[21] T. Liang, T. Shan, Y. Cheng, B.D. Devine, M. Noordhoek, Y. Li, Z. Lu, S.R. Phillpot and S.B. Sinnott, Classical atomistic simulations of surfaces and heterogeneous interfaces with the charge-optimized many body (COMB) potentials, *Mater. Sci. Eng. R Rep.* **74**, 2013, 255–279.

[22] X. Cui, Q.D. Zhang, X.Y. Li and F.Q. Zu, On crystallization behavior and thermal stability of Cu 64 Zr 36 metallic glass by controlling the melt temperature, *J. Non-Cryst. Solids* **452**, 2016, 336–341.

[23] P.H. Hünenberger, Thermostat Algorithms for Molecular Dynamics Simulations, 2005, Springer Berlin Heidelberg; Berlin, Heidelberg, 105–149.

[24] S. Plimpton, Fast Parallel algorithms for short-range molecular dynamics, *J. Comput. Phys.* **117**, 1995, 1–19.

[25] S. Alexander, Visualization and analysis of atomistic simulation data with OVITO-the Open Visualization Tool, *Model. Simul. Mater. Sci. Eng.* **18**, 2010, 015012.

[26] Z. Sha, P.S. Branicio, H.P. Lee and T.E. Tay, Strong and ductile nanolaminate composites combining metallic glasses and nanoglasses, *Int. J. Plast.* **90**, 2017, 231–241.

[27] L. Tian, Y. Cheng, Z. Shan, J. Li, C. Wang, X. Han, J. Sun and E. Ma, Approaching the ideal elastic limit of metallic glasses, *Nat. Commun.* **3**, 2012.

[28] W.H. Wang, The elastic properties, elastic models and elastic perspectives of metallic glasses, *Prog. Mater. Sci.* **57**, 2012, 487-656.

[29] M. Zhang, D. Yao, X. Wang and L. Deng, Air oxidation of a Zr55Cu30Al10Ni5 bulk metallic glass at its super cooled liquid state, *Corros. Sci.* **82**, 2014, 410–419.

[30] M. Zhang, L. Deng, D. Yao, J. Jin and X. Wang, Multilayered scale formation during Zr-based metallic glass oxidation in the supercooled liquid region, *Corros. Sci.* **111**, 2016, 556–567.

[31] S.H. Nandam, Y. Ivanisenko, R. Schwaiger, Z. Śniadecki, X. Mu, D. Wang, R. Chellali, T. Boll, A. Kilmametov, T. Bergfeldt, H. Gleiter and H. Hahn, Cu-Zr nanoglasses: atomic structure, thermal stability and indentation properties, *Acta Mater.* **136**, 2017, 181–189.

[32] Z.D. Sha, L.C. He, Q.X. Pei, H. Pan, Z.S. Liu, Y.W. Zhang and T.J. Wang, On the notch sensitivity of CuZr nanoglass, *J. Appl. Phys.* **115**, 2014, 163507.

[33] Y.Q. Cheng, A.J. Cao and E. Ma, Correlation between the elastic modulus and the intrinsic plastic behavior of metallic glasses: the roles of atomic configuration and alloy composition, *Acta Mater.* **57**, 2009, 3253–3267.

[34] X.L. Wang, F. Jiang, H. Hahn, J. Li, H. Gleiter, J. Sun and J.X. Fang, Plasticity of a scandium-based nanoglass, *Scripta Mater.* **98**, 2015, 40–43.

[35] H. Gleiter, Nanoglasses: a new kind of noncrystalline material and the way to an age of new technologies?, *Small* **12**, 2016, 2225–2233.

[36] A.S. Argon, Plastic deformation in metallic glasses, *Acta Metall.* **25**, 1979, 407–415.

[37] N. Li, L. Liu, Q. Chen, J. Pan and K.C. Chan, The effect of free volume on the deformation behaviour of a Zr-based metallic glass under nanoindentation, *J. Phys. D Appl. Phys.* **40**, 2007, 6055–6059.

[38] B. Xu, M.L. Falk, J.F. Li and L.T. Kong, Predicting shear transformation events in metallic glasses, *Phys. Rev. Lett.* **120**, 2018, 125503.

[39] T.C. Hufnagel, C.A. Schuh and M.L. Falk, Deformation of metallic glasses: recent developments in theory, simulations, and experiments, *Acta Mater.* **109**, 2016, 375–393.

[40] Y. Luo, Comprehensive Handbook of Chemical Bond Energies, 2007, CRC Press; Boca Raton.

[41] F. Faupel, W. Frank, M. Macht, H. Mehrer, V. Naundorf and K. R Tzke, Diffusion in metallic glasses and supercooled melts, *Rev. Mod. Phys.* **75**, 2003, 237–280.

[42] X. Wang, M. Zhang and L. Deng, Oxidation behavior of Zr55Cu30Al10Ni5 BMG under static loading, *J. Non-Cryst. Solids* **469**, 2017, 7–13.

Appendix A. Supplementary data

The following is the Supplementary data to this article:

Multimedia Component 1

Multimedia component 1

alt-text: Multimedia component 1

Graphical abstract

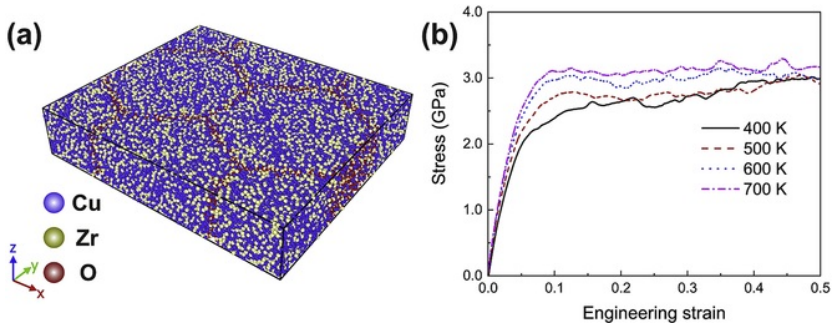

alt-text: Image 1

Highlights

- A novel NG consisting of glassy nano-cells connected by glassy oxide interfaces is proposed.
- The novel NG exhibits a superior combination of ultrahigh strength and ductility.
- Massive STZs are promoted to form in the vicinity of the oxide interface.
- Shear transformation is strictly confined in the interior of glassy cells.